A fully coupled transport-reaction model for a solid oxide fuel cell

Sanjay Kumar

A Thesis Submitted to

Indian Institute of Technology Hyderabad

In Partial Fulfillment of the Requirements for

The Degree of Master of Technology

भारतीय प्रौद्योगिकी संस्थान हैदराबाद

Indian Institute of Technology Hyderabad

Department of Chemical Engineering

June 2013

Declaration

I declare that this written submission represents my ideas in my own words, and where ideas or words of others have been included, I have adequately cited and referenced the original sources. I also declare that I have adhered to all principles of academic honesty and integrity and have not misrepresented or fabricated or falsified any idea/data/fact/source in my submission. I understand that any violation of the above will be a cause for disciplinary action by the Institute and can also evoke penal action from the sources that have thus not been properly cited, or from whom proper permission has not been taken when needed.

Sanjay kr

(Signature)

SANJAY KUMAR

(Sanjay Kumar)

CH11M13

(Roll No.)

Approval Sheet

This Thesis entitled **A fully coupled transport-reaction model for a solid oxide fuel cell** by Sanjay Kumar is approved for the degree of Master of Technology from IIT Hyderabad

(Dr. Parag D Pawar) Examiner
Dept. of Chem Eng
IITH

(Dr. Vinod Janardhanan) Examiner
Dept.of Chem Eng
IITH

(Dr. Dayadeep Monder) Adviser
Dept. of Chem Eng
IITH

(Dr. Kamakshi Jagannathan) External Examiner
COMSOL

(Dr. Karthik Ramanathan) External Examiner
Applied Materials

Acknowledgements

First and foremost, I would like to express my sincere gratitude to my supervisor Dr. Dayadeep Monder who gave me the opportunity to do this wonderful project, and helping me learn how to do research. I also learnt many new things which were unrelated to the project.

I am also grateful to the Department of Chemical Engineering, IIT Hyderabad and the other members of my supervisory committee: Dr. Ashok Kumar Pandey, Dr. Vinod Janardhanan, Dr. Parag D. Pawar.

I would like to express my gratitude to all those people who helped and supported me during the course of this M.Tech program at Indian Institute of Technology, Hyderabad.

THANKS AGAIN TO ALL WHO HELPED ME

Dedication

To my family

Abstract

Solid oxide fuel cells (SOFCs) are capable of the highest efficiency among energy conversion devices. Another advantage for SOFCs is the promise of fuel flexibility with full-scale prototypes running on natural gas and lab scale demonstrations of the direct use of higher hydrocarbons such as diesel. We are developing first principles models that describe the transport and reaction processes in a working SOFC with the aim of using these models for the design and optimization of such fuel cells. In this dissertation I developed 2D and 3D model for a planar Solid Oxide Fuel Cell. The current model includes fluid flow in porous electrodes and channels by solving Navier-Stokes equation in channels and Brinkman equation in porous electrodes. Species balance includes porous electrodes and channels by solving Maxwell-Stefan diffusion and convection relation. Charge transport is calculated in porous electrodes by solving Poisson's equation followed by modified Butler-Volmer equation. The model also considers detailed calculation of effective conductivity of composite electrodes anode (Ni-YSZ) and cathode (YSZ-LSM). The main aim of my thesis is to develop 2D and 3D models, in order to study the performance of these models with change in various parameters. In this work I use COMSOL Multiphysics to model the resulting fully coupled transport-reaction model for a anode-supported planar SOFC.

Contents

Declaration i

Approval Sheet i

Acknowledgements iv

Abstract vi

Nomenclature **viii**

1 Introduction **6**

1.1 Fuel cells 6

1.2 Solid Oxide Fuel Cells 8

1.2.1 Anode 8

1.2.2 Cathode 9

1.2.3 Electrolyte 9

1.3 Scope and plan of thesis 9

2 Physics of Solid Oxide Fuel Cells **10**

2.1 SOFC Thermodynamics 10

2.1.1 Gibbs free energy calculation 10

2.1.2 Relation between Gibb's free energy and voltage 10

2.1.3 Nersnt Equation 11

2.2 SOFC reaction kinetics 11

2.3 Mass transport in SOFCs 12

2.4 Voltage losses in an SOFC 13

2.4.1 SOFC efficiency 14

2.5 SOFC models in the literature 14

3 Multiphysics model for a SOFC **17**

3.1 Flow in gas channels and electrodes 18

3.1.1 Boundary conditions 19

3.2 Mass Transfer in the channels and electrodes 19

3.2.1 Boundary conditions 20
3.3 Voltage and Current Distribution 20
3.3.1 Boundary conditions 21
3.3.2 Effective conductivity 21
3.3.3 Current generation 22
3.4 Solver and meshing 24

4 Results and discussion **26**
4.1 Results from 3D model: current generation only at electrode-electrolyte boundaries 26
4.2 2D model results: current generation throughout electrodes 30

5 Conclusions **40**

List of Figures

1.1 A basic solid oxide fuel cell schematic [12] 7

3.1 Solid Oxide Fuel Cell: 2D geometry 18

3.2 Solid Oxide Fuel Cell: 3D geometry 18

3.3 Mesh for 2D geometry 24

3.4 Mesh for 2D geometry 24

4.1 Voltage and power density *vs* current density curves for 3D model. $x_{H_2,in} = 0.97$, $x_{H_2O,in} = 0.03$. 26

4.2 Effect of changing H_2 and H_2O content in fuel. 27

4.3 Effect of changing H_2 content in fuel, $x_{H_2O,in} = 0.03$. 28

4.4 Oxygen concentration along the channel and electrode 29

4.5 Hydrogen concentration along the channel and electrode 29

4.6 Changing electrolyte thickness 30

4.7 Effect of changing electrode porosity on cell performance. Inlet composition of fuel: 97% H_2 and 3% H_2O. 31

4.8 Effect of changing fuel flow rate on $V - i$ performance. Inlet composition of fuel: 97% H_2 and 3% H_2O. 32

4.9 Different air flow rate 33

4.10 x_{H_2}in fuel, x_{O_2} in air, and i profiles along the length of the cell. $V_{cell} = 0.3V$; counter-flow of air and fuel. Inlet composition of fuel: 97% H_2 and 3% H_2O. . . . 34

4.11 x_{H_2}in fuel, x_{O_2} in air, and i profiles along the length of the cell. $V_{cell} = 0.3V$; co-flow of air and fuel. Inlet composition of fuel: 97% H_2 and 3% H_2O. 35

4.12 x_{H_2}in fuel, x_{O_2} in air, and i profiles along the length of the cell. $V_{cell} = 0.8V$; counter-flow of air and fuel. Inlet composition of fuel: 97% H_2 and 3% H_2O. . . . 36

4.13 x_{H_2}in fuel, x_{O_2} in air, and i profiles along the length of the cell. $V_{cell} = 0.8V$; co-flow of air and fuel. Inlet composition of fuel: 97% H_2 and 3% H_2O. 37

4.14 Cell performance as a function of anode thickness t_{anode}. Inlet composition of fuel: 97% H_2 and 3% H_2O. 38

4.15 Cell performance as a function of cathode thickness t_{anode}. Inlet composition of fuel: 97% H_2 and 3% H_2O. 39

.

List of Tables

3.1 Simulation conditions used in the porous anode model 23
3.2 Parameters used in the model 24

.

Nomenclature

B_g	permeability, (cm^2)
D_{ki}	binary diffusion coefficient (cm^2/s)
d_p	particle diameter(cm)
E_{a,H_2}	activation energy for H_2 oxidation,(J/mol)
E_{a,O_2}	activation energy for O_2 reduction,(J/mol)
E_a^{eq}	equilibrium electric-potential difference in the anode,(V)
E_c^{eq}	equilibrium electric-potential difference in the cathode,(V)
F	Faraday constant,(C/mol)
I	identity matrix
i	current density vector(A/cm^2)
i_o	exchange current density (A/cm^2)
$i_{o,a}$	exchange current density for H_2 oxidation (A/cm^2)
$i_{o,c}$	exchange current density for O_2 reduction (A/cm^2)
$i^*_{H_2}$	parameter in the expression of $i_{o,a}$ (A/cm^2)
$i^*_{O_2}$	parameter in the expression of $i_{o,c}$ (A/cm^2)
i^*_{ref,H_2}	parameter $i^*_{H_2}$ at the reference temperature T_{ref} (A/cm^2)
i^*_{ref,O_2}	parameter $i^*_{O_2}$ at the reference temperature T_{ref} (A/cm^2)
j_i	diffusive flux mol/cm^2s
M_i	molar mass of given species (g/mol)
n	normal vector
p	pressure (atm)
p_{H_2}	partial pressure of H_2 (atm)
p_{O_2}	partial pressure of O_2 (atm)
p_{H_2O}	partial pressure of H_2O (atm)
$p^*_{H_2}$	parameter in the expression of $i_{o,a}$ (atm)
$p^*_{O_2}$	parameter in the expression of $i_{o,c}$ (atm)
p_α	probability of α particles
R	universal gas constant $(J/molK)$
r_{ed}	radius of electrode particle (cm)
r_{el}	radius of electrolyte particle (cm)
T	Temperature (K)
v	mass average velocity vector
w_k	species molecular weight (g/mol)
Z_{ed}	coordination number of the electrode particles
Z_{el}	coordination number of the electrolyte particles
Z_α	coordination number of α particles
Z_β	coordination number of β particles
$Z_{\alpha,\beta}$	coordination number of α, β particles

Greek latter

μ	Viscosity (Kg m^{-1} s^{-1})
ρ	Density (kg m^{-3})
τ	Tortuosity
η_{act}	activation losses
η_{con}	concentration losses
η_{ohmic}	ohmic losses
ϕ_g	porosity
γ	Bruggeman factor
$\gamma_\circ$	sticking coefficients
α	charge transfer coefficient
Γ	surface site density, (mol/cm^2)
σ°_{LSM}	electric conductivity of pure LSM, (S/cm)
σ°_{Ni}	electric conductivity of pure Ni, (S/cm)
σ°_{YSZ}	electric conductivity of pure YSZ, (S/cm)
ψ_{ed}	volume fraction of electrode particles in solid phase
ψ_{el}	volume fraction of electrolyte particles in solid phase
$\mu^\circ_{H_2}$	standard state chemical potential of $H_2, (J/mol)$
$\mu^\circ_{H_2O}$	standard state chemical potential of $H_2O, (J/mol)$
$\mu^\circ_{O_2}$	standard state chemical potential of $O_2, (J/mol)$
ζ_{ed}	number fraction of the electrode particles
ζ_{el}	number fraction of the electrolyte particles
ϕ_{ed}	electronic-conducting particle volume fraction
ϕ_{el}	ionic-conducting particle volume fraction

Chapter 1

Introduction

1.1 Fuel cells

The world's increasing need for electrical energy is driven by 1) an increase in population, and 2) rising energy demand per capita from developing nations. One of most important problems facing us today is the need to design energy systems that can satisfy this increasing demand for energy in a sustainable manner that is, without contributing to greenhouse gas emmissions. Fuel cell is one among several other technologies including Solar, Wind, Biofuels, etc. that will need to be developed in order to satisfy the urgent need for sustainable energy.

Fuel cells are electrochemical devices that directly convert chemical energy into electrical energy through chemical reaction of a fuel with oxygen [18]. The most important feature of fuel cells in the context of sustainable energy is their intrinsically higher energy conversion efficiency. Batteries and fuel cells operate on the same principle by converting chemical energy into electrical energy with the difference being that fuel cells can utilize a constant source of fuel (with continuously available oxygen) to produce electricity continually for as long as these inputs are supplied. Fuel cells can be built and operated to satisfy a wide range of electrical power requirements from a few milli watts to several mega watts. The product from the fuel cell is water and heat, water is vaporized due to operating at very high temperature $600 - 1000^oC$ and heat again utilized in the heat the water and other uses also.

One could say fuel cell research started in the late 1830s when German physicist Christian Friendrich Schonbein and Welsh physicist William Grove invented the first fuel cells [26]. The first important use of fuel cells was in the NASA space program to generate power for probes, satellites and space capsules.

A fuel cell is made up of three components: a porous electrode called the anode where the oxidation of fuel takes place, an electrolyte across which the ions are transported and, a second porous electrode called the cathode where the reduction of oxygen (typically supplied as air) takes place. Figure 1.1 shows a solid oxide fuel cell schematic diagram which can help understand the basic working of a fuel cell. Both the gaseous fuel as well as the oxidant (usually air) are fed continuously to the electrodes. At the anode (negative electrode), the fuel is oxidized while the oxygen is reduced at the cathode. To complete the reaction as well as the electrical circuit, the

charged species (ions and electrons) produced at one electrode have to make their way to the other electrode. The ions can only travel through the electrolyte while the electrons have to travel through the external circuit through the electrical load. The overall reaction (with H_2 as fuel) produces water and heat.

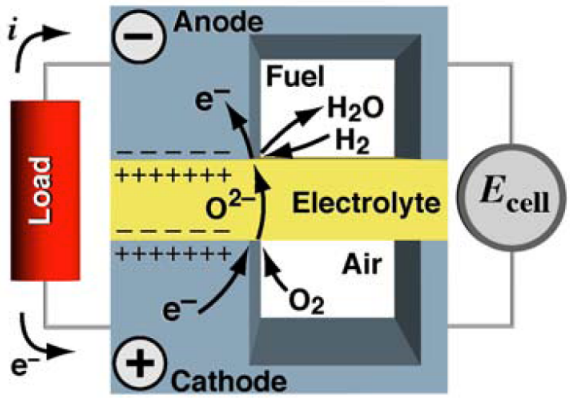

Figure 1.1: A basic solid oxide fuel cell schematic [12]

There are many advantages of using fuel cells but the main advantage is their exceptionally high efficiency of energy conversion. Their ability to produce electricity directly from chemical energy plays a part in their higher efficiency of energy conversion. There are no moving parts in fuel cell so it is mechanically idle. So fuel cells do not make any noise in working conditions and emission of undesirable products such as NOx, SOx and particulate is negligible because no direct combustion takes place inside a fuel cell. As mentioned earlier, fuel cells are highly scalable and can satisfy a broad range of power requirements. One disadvantage of fuel cells is fuel availability and storage especially in the context of hydrogen as fuel.

Fuel cells are categorized into five major types, out of these some are already commercialized and other types are closed to commercialization.

1 Alkaline fuel cell (AFC)

2 Phosphoric acid fuel cell (PAFC)

3 Polymer electrolyte membrane fuel cell (PEMFC)

4 Solid oxide fuel cell (SOFC)

5 Molten carbonate fuel cell (MCFC)

All of the above are classified based on the electrolyte used. Other factors that play a role once the electrolyte is chosen include fuel compatibility, operating temperature, etc. This work focuses on solid oxide fuel cells and a brief description of SOFCs and a literature review of SOFC models is given in the following section.

1.2 Solid Oxide Fuel Cells

A solid oxide fuel cell is a fuel cell with a oxide ion conducting ceramic electrolyte. These electrolytes only achieve appreciable ionic conductivities at elevated temperatures of $600 - 1000°C$. Solid oxide fuel cells (SOFCs) are capable of the highest efficiency among energy conversion devices. Another advantage for SOFCs is the promise of fuel flexibility with full-scale prototypes running on natural gas and lab scale demonstrations of the direct use of higher hydrocarbons such as diesel. Thus, SOFCs can be operated with a variety of fuels, including hydrogen, CO, hydrocarbons or mixture of these. Additionally, unlike low temperature fuel cells where Pt and other precious metal catalysts are required for the electrodes, a much cheaper set of materials can be used as catalysts in SOFCs. These advantages of SOFCs are linked to the high operating temperatures required due to the electrolytes used. There are disadvantage of this high operating temperature as well e.g., longer start-up times, and mechanical, and chemical compatibility issues between the different layers/materials inside a solid oxide fuel cell.

Figure 1.1 represents a single solid oxide fuel cell. If we start from the fuel channel (upper section labelled Fuel), the fuel has to be transported to the reaction sites which lie at the interface of the fuel, anode catalyst, and electrolyte materials. These interfacial active sites are called the three phase bounday (tpb). The fuel reacts with oxide ions in the electrolyte giving water vapour and electrons as see in reaction 1.1. The electrons travel through the external circuit driving the electrical load. On the other side, the oxygen in the air channel has to reach the reaction sites on the tpb sites in the cathode. The oxygen then reacts, consuming electrons, to give oxide ions as shown by reaction 1.2. These oxide ions travel through the electrolyte to the anode side to complete the circuit and the overall reaction. Further explanation of SOFC operation is not given here as the following chapters will detail the physics and mathematical modeling of SOFC operation.

$$\mathrm{H_2 + O^{2-} \rightarrow H_2O + 2e^-} \tag{1.1}$$

$$\mathrm{O_2 + 4e^- \rightarrow 2O^{2-}} \tag{1.2}$$

A brief description follows of the three main layers/components in a SOFC:

1.2.1 Anode

The most common anode used is a porous layer of composite Ni catalyst and yttria-stabilized zirconia (YSZ). This cermet (composite ceramic and metal) is an ionic and electronic conducting material and because of the porosity, gas phase species can also be transported through it. Ni is used because it is a very good electrocatalyst for the oxidation reaction and a good electronic conductor. The composite structure which is composed of micron scale Ni and YSZ particles has electrochemically active three phase boundary sites throughout. As mentioned earlier, the oxidation reaction occurs at these tpb sites. In most current designs, the anode layer is the thickest in the fuel cell and provides mechanical support to the cell. These thicker anodes offer significant Ni surface area which can be utilized for fuel reforming should the cell design need it.

1.2.2 Cathode

The most common cathode is a porous composite mixture of LSM (lanthanum strontium manganite) and YSZ (yttria-stabilized zirconia). LSM is a mixed oxide ceramic material generally denoted as $La_{1-x}Sr_xMnO_3$, where x describes the doping level x varies from 10 to 20 percent. At SOFC operating temperatures LSM has a high electric conductivity and low ionic conductivity. Like the anode, the cathode is also designed to be a mixed ionic-electronic conductor with low resistance to gaseous oxygen transport, and a substantial number of tpb sites for the reduction reaction. A different set of materials is recommended for operating temperatures less than about $750°C$.

1.2.3 Electrolyte

The electrolyte materials used in SOFCs are ceramic mixed metal oxides and the most popular SOFC electrolyte is YSZ which is used almost exclusively in designs operating above $\approx 750°C$. The most important characteristics for an SOFC electrolyte are low ionic resistivity, very high electronic resistivity, and good chemical stability in highly oxidizing as well as reducing atmospheres. The electrolyte is usually a very thin layer to minimize Ohmic losses.

1.3 Scope and plan of thesis

This work focusses on building multiphysics models for an operating SOFC. These 2D and 3D models incorporate various transport processes and the electrochemistry in an SOFC into account by solving the associated partial differential equations (PDEs). These processes and thus the PDEs are strongly coupled to one another which makes solution of the full problem difficult.

In this work, we first develop the above detailed models and then use them to perform a series of parametric studies that help us better understand the coupling of the various physics. The ultimate aim in building these models is to use them for SOFC cell and stack design and optimization studies.

Chapter 2 presents brief desciptions of the various physics in an operating SOFC and outlines the performance loss mechanisms. A short review of the SOFC modeling literature is also given in chapter 2. Chapter 3 presents the details of the models used in this work including the differential equations, the boundary conditions, and the solution methods used. In chapter 4 we report the results of a number of parametric studies that help us understand the potential and limitations of a single planar anode supported SOFC.

Chapter 2

Physics of Solid Oxide Fuel Cells

In this chapter we are going to briefly outline the various physics that need to be taken into account while modeling a solid oxide fuel cell. These include: thermodynamics which dictates the maximum theoretical cell voltage, charge transport and mass transport through the electrodes and electrolyte, and electrochemical reaction kinetics. Heat generation and transport is not considered in this work and the models built are isothermal. After introducing the above physics, we briefly outline the voltage losses in a fuel cell to show how the finite rate of the transport and kinetic processes leads to these losses.

2.1 SOFC Thermodynamics

This section outlines the relationship between Gibbs free energy and the maximum electrical potential for the cell: the Nernst equation.

2.1.1 Gibbs free energy calculation

Gibbs free energy $\triangle g$ is the work potential of a reaction and can be calculated using equation (2.1) which relates $\triangle g$ to the change in enthalpy and entropy for the reaction.

$$\triangle g = \triangle h - T \triangle s \tag{2.1}$$

2.1.2 Relation between Gibb's free energy and voltage

The work done by a fuel cell is electrical work thus equation (2.2) holds which leads to equation (2.4). Here q is the charge transferred, F is Faraday's constant, n is the number of electrons transferred in the reaction, and E is the potential for electrical work as measured by the electric potential.

$$W = qE \tag{2.2}$$
$$q = nF \tag{2.3}$$
$$W = nFE \tag{2.4}$$

From the first law of thermodynamics $\Delta h = Q - W$ for a reversible process gives equation (2.6). Rearranging (2.6), we get (2.7), which is equivalent to the Nernst equation (2.8) where E is the reversible voltage for the reaction.

$$Q = T\Delta s \tag{2.5}$$
$$\Delta h = T\Delta s - nFE \tag{2.6}$$
$$\Delta h - T\Delta s = \Delta g = -nFE \tag{2.7}$$
$$E = \frac{-\Delta g}{nF} \tag{2.8}$$

If the reactants and products are in their standard states then equation (2.8) becomes:

$$E^\circ = \frac{-\Delta g^\circ_{rxn}}{nF} \tag{2.9}$$

The variation of the reversible voltage with temperature T can be calculated as:

$$E^\circ(T) = E^\circ(T^\circ) + \frac{\Delta s^\circ}{nF}(T - T^\circ) \tag{2.10}$$

If Δs° is negative (hydrogen fuel cell), $E^\circ(T)$ decreases with an increase in T.

2.1.3 Nersnt Equation

Equation (2.8) when written as an explicit function of reactant and product activities/concentrations is known as the Nernst equation (2.11).

$$E = E^\circ - \frac{RT}{nF} ln \frac{\prod a^{\nu_i}_{products}}{\prod a^{\nu_i}_{rectants}} \tag{2.11}$$

This equation relates the equilibrium potential E to the standard potential E° (2.9), temperature, and the pressure/concentrations of the reactants and products.

2.2 SOFC reaction kinetics

Although thermodynamics dictates a maximum/reversible cell voltage, the voltage of an operating fuel cell is always lower than this Nernst voltage. One of the reasons for this is that the electrochemical reactions at each electrode require a finite potential difference to generate current. The current generation is directly proportional to the rate of electrochemical reaction according

to equation (2.12), where r_i is the molar rate of reaction for species i and n_i is the number of electrons released/consumed per molecule of i, I is the current, and $F = 96485$ C/mole is Faraday's constant.

$$r_i = \frac{I}{n_i F} \tag{2.12}$$

The current generated is usually calculated using phenomenological equations such as the Butler-Volmer equation [18]. One form of the Butler-Volmer equation [16] written for the hydrogen electro-oxidation reaction, reaction (1.1), on the anode is given by equation (2.13).

$$i = i_{0_{in}} \left\{ \frac{C_{H_2}}{C_{H_{2,in}}} e^{-\frac{\alpha F}{RT}\eta_{in}} - \frac{C_{H_2O}}{C_{H_2O,in}} e^{\frac{(1-\alpha)F}{RT}\eta_{in}} \right\} \tag{2.13}$$

Where i is the current density defined as $i = \frac{I}{A}$ where A is the apparent area of the electrode where the current is generated, $i_{0_{in}}$ is called the exchange current density and is a function of T and the inlet fuel composition. C_{H_2} is the concentration of H_2 and C_{H_2O} is the concentration of H_2O, α is the symmetry or charge transfer coefficient and $\eta_{in} = E - E_{in}$ is the anode activation overpotential. E is the operating anode potential and E_{in} is the equilibrium anode potential at fuel inlet conditions (2.14).

$$E_{in} = E^{\circ} + \frac{RT}{2F} \ln \frac{C_{H_2,in}}{C_{H_2O,in}} \tag{2.14}$$

Thus, the Butler-Volmer equation describes how current and voltage are related for an electrochemical reaction. This equation shows how the current produced by an electrochemical reaction increases exponentially with activation overvoltage.

2.3 Mass transport in SOFCs

Mass transport plays an important role in deciding the performance of any particular design of fuel cell. To maintain a required current, an equivalent amount of fuel needs to make its way to the active reaction sites (tpb) in the anode. The easier this species transport through the fuel channel and anode, the higher the concentration of the fuel at the reaction sites and the higher the concentration, the better the performance as seen clearly by looking at equation (2.13) above. The same argument also holds for the transport of oxygen through the air channel and cathode to the active sites/tpb in the cathode.

In general, convective mass transfer dominates in the fuel and air channels and diffusive mass transfer dominates in the electrodes. Thus, the cell performance will be better for higher flow-rates and more permeable electrodes. While flow-rates are dictated by fuel/air utilization and thus cannot be increased beyond a certain range, electrode design is critical to minimize the mass transfer limitations.

As mentioned above, the mass transfer in SOFC electrodes is dictated by diffusion. Typically the electrode thickness is much smaller than that of the flow channel. Inside the flow channels,

the resistance to mass transfer is much lower and the active species concentration is more or less constant while the active species concentrations in the electrodes can have sharp gradients.

2.4 Voltage losses in an SOFC

The voltage of an operating SOFC is always lower than the Nernst voltage due to voltage losses in the electrodes and electrolyte caused by reaction and transport limitations.

As in other fuel cells, the performance losses in an operating SOFC are: 1) Activation polarization(η_{act}), Ohmic polarization (η_{ohmic}), Concentration polarization (η_{conc}). Thus the operating voltage for a fuel cell can be expressed as (2.15).

$$V_{cell} = E - \eta_{act} - \eta_{ohmic} - \eta_{conc} \tag{2.15}$$

- **Activation losses** (η_{act}): Activation losses happen because of the finite rates of electrochemical reaction at the anode and cathode. The activation voltage loss or polarization is given by the Butler-Volmer equation (2.13). In the high current region or if the overpotential is high, (2.13) can be approximated by the Tafel equation (2.16).

$$\eta_{act} = -\frac{RT}{\alpha nF} \ln i_0 + \frac{RT}{\alpha nF} \ln i \tag{2.16}$$

  The Tafel equation is usually expressed in the generalized form below where b is called the Tafel slope.

$$\eta_{act} = a + b \ln i \tag{2.17}$$

- **Ohmic losses**(η_{ohmic}): Ohmic losses occur due to resistance to charge transport in the fuel cell. Although these losses occur in all three layers as well as the interconnects, the losses in the electrolyte are typically orders of magnitude higher. Thus, for most designs, the Ohmic voltage loss is given by equation (2.18), where $l_{electrolyte}$ is the thickness and σ_{ionic} is the ionic conductivity of the electrolyte.

$$\eta_{ohmic} = i \left(\frac{l_{electrolyte}}{\sigma_{ionic}} \right) = IR_{ionic} \tag{2.18}$$

- **Concentration losses**(η_{conc}):

  Concentration losses or the mass transfer losses are due to reactant depletion and product accumulation within the electrodes. In the simplest case, the concentration polarization is given by (2.19) where i_L is the limiting current density and given by (2.20). D^{eff} is the effective diffusivity, $C_{k,channel}$ is the concentration of the reacting species in the fuel or air channel, and $l_{electrode}$ is the thickness of the electrode. Thus, the cathode and anode will have seperate η_{conc} terms.

  A more detailed analysis will add more terms to (2.19) but the qualitative behaviour is the same.

$$\eta_{conc} = \frac{RT}{nF} \ln \frac{i_L}{i_L - i} \tag{2.19}$$

$$i_L = -D^{eff} nF \frac{C_{k,channel}}{l_{electrode}} \tag{2.20}$$

2.4.1 SOFC efficiency

Fuel cell efficiency is defined as the ratio of useful energy generated to the total energy used by the process. The thermodynamic efficiency or ideal efficiency is given by

$$\eta_{thermo} = \frac{\Delta g}{\Delta h} \tag{2.21}$$

Thermodynamic efficiency η_{thermo} of the hydrogen fuel cell decreases as temperature increases because the entropy of reaction is negative. Real fuel cell efficiency is always less than ideal thermodynamic efficiency because of transport and kinetic losses $\eta_{voltage}$ as well as fuel utilization losses η_{fuel}.

The real efficiency of a fuel cell can be calculated by

$$\eta_{real} = \eta_{thermo} \times \eta_{voltage} \times \eta_{fuel} = \frac{\Delta g}{\Delta h} \frac{V}{E} \frac{i}{(nF)\dot{n}_{fuel}} \tag{2.22}$$

Where V is the actual cell voltage, and $\dot{n}_{fuel}$ is the molar flow-rate of fuel supplied to the cell.

2.5 SOFC models in the literature

Several researchers have developed models to study SOFCs at various scales. Thus there are large number of models available that simulate processes from the molecular to the system levels. This work focuses on single cell models and we briefly mention some of the relevant models available in the literature. The models of interest to us are the ones that simulate the transport and reaction processes at the micron to millimeter scales.

Zhu et al. [27] developed one dimensional planar model and studied charge distribution through the electrodes, fluid flow along the channel and electrodes. Porous transport in the electrodes is represented by dusty gas model, charge-transfer chemistry is represented by a modified Butler-Volmer equation that is derived from elementary reaction. They considered methane reforming reaction and water gas shift reaction to produce hydrogen gas, this hydrogen gas fed in to the SOFCs as a inlet fuel. C++ with Cantera interface and Fortran with Chemkin interface were used to solve all the equations numerically. They presented current-voltage curve and compared that with the experimental results of Jiang and Virkar. At various mixture mole fractions, they showed the variation of current density, power along the channel length.

Zhu et al. [28] developed a model which included distributed-charge transfer to represent composite electrodes. The model was a fully coupled model of membrane electrode assembly (MEA)

i.e. anode, cathode and electrolyte. The charge transfer in the model was governed by modified Butler-Volmer relation. Dusty Gas Model(DGM) was used for evaluating mass fluxes of gas-phase species in porous structure and energy equation was solved in order to know the temperature profile through the membrane electrode assembly. Effective properties like conductivity within the porous structures are modeled using percolation theory. They used finite-volume approach to discretize the equation and differential-algebraic equations (DAEs) are solved using Limex software. The authors validated their result by comparing the charge-transfer chemistry and porous media properties with those obtained from various button-cell experiments. They presented current-voltage curve for different composition of hydrogen and water at constant temperature $800°C$.

Sanyal et al. [19] developed particle-resolved simulations to predict the effective conductivity within porous composite electrodes. In this work they used percolation theory to calculate the effective conductivity and by adjusting Bruggeman factor between 1.5 to 3.5 they calculated the resolved result of effective conductivity value in porous electrode.

DiGiuseppe et al.[8] in 2012 developed 2D model for planar model for SOFC cell. They used COMSOL Multiphysics software to model the fluid dynamics, electrochemistry, electrical conduction and diffusion physics. They validated own experiment data to model data.

Li et al. [14] in 2003 developed a 2D numerical model for the heat/mass transfer, fluid flow and chemical/electrochemical transport process in tubular solid oxide fuel cell (SOFC) in a stack. Their model predicted cell voltage with less than 7.4 % deviation from all experimental data. They also got satisfactory results in terms of fuel cell temperature. They validated their model with the works of Hagiwara et al. [10], Hirano et al. [11], Singhal et al. [20][21], Tomlins and Jaszar et al. [24]

Suwanwarangkul et al. [22] in 2003 presented a comparative study of the performance between Fick's model (FM), Stefan Maxwell model (SMM) and Dusty Gas model (DGM) to predict the concentration over-potential of a SOFC anode. All models were validated with the experimental data for $CO - CO_2$ and $H_2 - H_2O - Ar$ system. They concluded that dusty gas model is more appropriate model to simulate gas transport phenomena inside a SOFC anode. Dusty gas model requires numerical simulation where as in case of Fick's model and Stefan-Maxwell's model no numerical simulation is required. In the low current density limit, it was found that Stefan-Maxwell's model is a better approximation of the Dusty gas model than the Fick's model.

Kenney et al. [13] in 2009 developed a model for a solid oxide fuel cell composite electrode structure based on measurable starting parameter. This method allows to calculate all relevant electrode micro-structure parameters. They presented pore size, internal surface area, triple phase boundary length and percolation of all relevant phase in composite electrode. They found large particle size distribution reduces the triple phase boundary length. Also the average pore size was found to be of 0.19 μm.

Wilson et al. [25] in 2008 studied performance in anode supported SOFCs with changing Ni-YSZ and compared structurally using FIB-SEM. They found that the highest triple phase boundary density occurs at Ni:YSZ volume ratio of ~ 0.5. Polarization resistance was determined not only by TPB density but also by other factors such as tortuosity and contiguity.

Daifen et al. [5] in 2009 developed a micro-model based upon percolation theory to predict effective properties in composite electrodes for SOFC application. This micro-model predicts electronic and ionic conductivity, TPB lengths and hydraulic pore radii. The effective properties depend upon particle contact angles, porosity, average particle-radii, volumetric packing densities. They derived a formula to calculate the effective conductivity of the mixture component. The authors validated their result by comparing with the work of Suzuki and Oshima et al.[23].

Chapter 3

Multiphysics model for a SOFC

One can model SOFCs at many different length scales. In this thesis, we build models at the single cell scale and include physics at the micron to centimeter scales. These models simulate the operation of a planar anode-supported SOFC in 2D and 3D to examine and explain the role of a selected set of design parameters and operating conditions. In this chapter, we present a description of the models including the governing differential equations and boundary conditions used.

Figures 3.1 and 3.2 give the 2D and 3D model geometries. The following dimensions are used for the geometry: anode thickness $550\mu m$, cathode thickness $50\mu m$, electrolyte thickness $20\mu m$, channel area $1mm^2$ (channel height is 1 mm), and length of the channel $5cm$.

This model includes the following physics:

- Flow in the gas channels and electrodes
- Mass Transfer in the channels and electrodes
- Voltage and current distribution in the electrodes and electrolyte

Heat transfer is not considered in this work and the models and results are for isothermal operation at $800°C$.

Model geometry

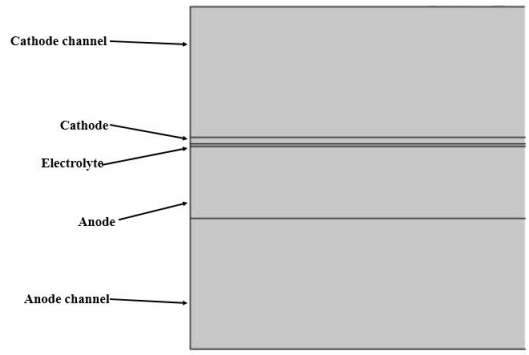

Figure 3.1: Solid Oxide Fuel Cell: 2D geometry

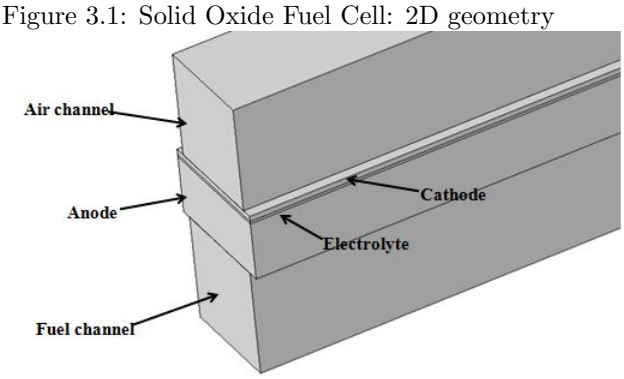

Figure 3.2: Solid Oxide Fuel Cell: 3D geometry

3.1 Flow in gas channels and electrodes

The fluid flow in the fuel and air channel is modeled using the weakly compressible form of the Navier-Stokes equations:

$$\rho\left(\mathbf{v}\cdot\nabla\right)\mathbf{v} = -\nabla\mathbf{p} + \nabla\cdot\left[\mu\left(\nabla\mathbf{v} + \left(\nabla\mathbf{v}\right)^{\mathbf{T}}\right) - \frac{\mathbf{2}}{\mathbf{3}}\mu\left(\nabla\cdot\mathbf{v}\right)\mathbf{I}\right] + \mathbf{F} \tag{3.1}$$

$$\nabla\cdot\left(\rho\mathbf{v}\right) = 0 \tag{3.2}$$

where $\mathbf{v}$ is velocity vector, μ is viscosity of fluid [15], ρ is the density, p is the pressure and I is the identity matrix.

$$\frac{\mu}{\kappa}\mathbf{v} = -\nabla\mathbf{p} + \frac{\mathbf{1}}{\epsilon}\nabla\cdot\left[\mu\left\{\nabla\mathbf{v} + \left(\nabla\mathbf{v}\right)^{\mathbf{T}}\right\} - \frac{\mathbf{2}}{\mathbf{3}}\mu(\nabla\cdot\mathbf{v})\mathbf{I}\right] \tag{3.3}$$

$$\nabla\cdot\left(\rho\mathbf{v}\right) = S_m \tag{3.4}$$

κ is the permeability of the porous electrode and ε_p is the porosity. S_m is the mass source term

equivalent to the current generated. This term is non-zero only if volumetric current generation is allowed (as opposed to current generation only at the boundary of the electrodes and electrolyte).

The permeability is calculated by the Kozeny-Carman relation[1]:

$$\kappa = \frac{{\phi_g}^3 d_p^2}{72\tau_g \left(1-\phi_g\right)^2} \tag{3.5}$$

3.1.1 Boundary conditions

- Mass flow rate is specified at inlet of air and fuel side.
- Gauge pressure is zero at both fuel and air exit.
- No slip boundary condition at the walls.

$$v = 0|_{\partial\Omega walls} \tag{3.6}$$

- Mass flux due to electrochemical reaction at the electrode-electrolyte boundaries. This BC appears if the current generation is only allowed at the electrode-electrolyte boundary (as opposed to volumetric current generation throughout the electrode).

3.2 Mass Transfer in the channels and electrodes

The mass transfer equation or the convection-diffusion equation tracks the concentration for all gas phase species in the fuel/air channels and electrodes.

$$\nabla \cdot j_i + \rho \left(\mathbf{v} \cdot \nabla\right) w_i = r_i \tag{3.7}$$

Where w_i is the mass fraction and r_i is the mass source/sink term. r_i is non-zero only if current generation is allowed throughout the electrodes. The diffusive flux is given by the Maxwell-Stefan equation [17] and [2].

$$j_i = -\sigma w_i \sum_{k=1}^{n} D_{ik} \left[\nabla y_k + \left(y_k - w_k\right)\frac{\nabla p}{p}\right] \tag{3.8}$$

Where n is the total number of species in the mixture, D_{ik} is the multicomponent diffusivity for species i in a mixture with species k given by the Fuller, Schettler, and Giddings equation below [7].

$$D_{ik} = \frac{10^{-7} T^{1.75} \sqrt{10^3 \frac{M_i + M_k}{M_i M_k}}}{p\left[\left(\sum v_i\right)^{\frac{1}{3}} + \left(\sum v_k\right)^{\frac{1}{3}}\right]} \tag{3.9}$$

Where M_i and M_k are the molar masses, $\sum V_i$ and $\sum V_k$ the diffusion volumes for the components i and k. T is temperature in K and P is the pressure in atm.

The gas species diffusivity in the electrodes needs to be adjusted for porosity as well as tortuosity and the effective diffusivity is defined as:

$$D_{ik,eff} = \frac{\varepsilon}{\tau_g} D_{ik} \tag{3.10}$$

Where ε is the porosity and τ_g is the tortuousity[28] of the pores in the electrode.

3.2.1 Boundary conditions

1. Mass fraction of H_2 in fuel and O_2 in air is specified at the fuel channel inlet and air channel inlet respectively.

$$w_{H2}|_{\partial\Omega_{fuel,inlet}} = w_{H2,in} \tag{3.11}$$

$$w_{O2}|_{\partial\Omega_{air,inlet}} = w_{O2,in} \tag{3.12}$$

2. No flux set at the walls of the channels

$$n \cdot J_i|_{\partial\Omega_{wall}} = 0 \tag{3.13}$$

3. Species mass flux due to electrochemical reaction at electrode-electrolyte boundaries if current generation is only allowed at the electrode-electrolyte boundary .

3.3 Voltage and Current Distribution

The electronic and ionic potentials in the electrodes and electrolyte are modeled using the vector form of Ohm's law given by Poisson's equation. Thus equation (3.14) gives the ionic potential in the electrolyte and (3.15) and (3.16) gives the ionic and electronic potential in the composite electrodes.

$$\nabla \cdot (-\sigma_i \nabla \phi_i) = 0 \tag{3.14}$$

$$\nabla \cdot (-\sigma_i^{eff} \nabla \phi_i) = i_V \tag{3.15}$$

$$\nabla \cdot (-\sigma_e^{eff} \nabla \phi_e) = -i_V \tag{3.16}$$

where ϕ_i is ionic potential, ϕ_e is the electronic potential, σ_i is the ionic conductivity of the electrolyte, σ_i^{eff} is the effective ionic conductivity, and σ_e^{eff} the effective electronic conductivity of the electrodes. i_V is the volumetric current generation in the electrodes.

3.3.1 Boundary conditions

- Electric insulation or no flux at the electrode and electrolyte edges.

$$\mathbf{n} \cdot (\nabla \phi) = 0 \tag{3.17}$$

- Electric ground specified at the current collector of the anode i.e $\phi_e = 0$
- Electric potential specified at the current collector of the cathode i.e $\phi_e = V_{cell}$
- Current density due to electrochemical reaction at the electrode-electrolyte interfaces (if not considering volumetric current generation).

3.3.2 Effective conductivity

To solve equations 3.15 – 3.16 the values of the effective conductivity for both ionic and electronic transport through the porous composite electrodes need to be calculated [4]

Effective conductivity of composite electrodes, Ni-YSZ and LSM-YSZ, is determined using percolation and co-ordination number theory [3, 9, 28]. Some of the details for the calculation of effective conductivity are given below:

$$\sigma_\alpha^{eff} = \sigma_\alpha^0 \left[(1 - \phi_g) \, \psi_\alpha P_\alpha \right]^\gamma \tag{3.18}$$

Where σ_α^0 is conductivity of phase α in the composite electrodes. The conductivities (S/cm) of Ni and LSM are given by:

$$\sigma_{Ni}^0 = \frac{8.855 \times 10^5}{T} exp\left(-\frac{9000}{RT}\right) \tag{3.19}$$

$$\sigma_{LSM}^0 = 3.27 \times 10^4 - 10.653T \tag{3.20}$$

ϕ_g is the porosity of anode and cathode, ψ_α and P_α are volume fraction and percolation threshold of phase α, and $\gamma = 3.5$ is the Bruggeman factor.

According to Suzuki and Oshima [23], the percolation threshold for phase α can be determined using equation (3.21)

$$P_\alpha = \left[1 - \left(\frac{4.236 - Z_{\alpha\alpha}}{2.472} \right)^{2.5} \right]^{0.4} \tag{3.21}$$

$Z_{\alpha\alpha}$ is the number of ionic and electronic particle neighbors and calculated as:

$$Z_{\alpha\beta} = \zeta_\beta \frac{Z_\alpha Z_\beta}{Z_{tot}} \tag{3.22}$$

Where Z_{tot} is the overall average coordination number($Z_{tot} = 6$ in a random packing of binary sphere).

The coordination numbers for the ionic and electronic conducting composite electrode can be calculated by

$$Z_{ed} = 3 + \frac{(Z_{tot} - 3)r_{ed}^2}{\zeta_{ed} r_{ed}^2 + \zeta_{el} r_{el}^2} \tag{3.23}$$

$$Z_{el} = 3 + \frac{(Z_{tot} - 3)r_{el}^2}{\zeta_{ed} r_{ed}^2 + \zeta_{el} r_{el}^2} \tag{3.24}$$

The number fraction of the electrode and electrolyte particle ζ_{ed} and ζ_{el} calculated as:

$$\zeta_{ed} = \frac{\psi_{ed} r_{ed}^3}{\psi_{ed} r_{ed}^3 + \psi_{el} r_{el}^3} \tag{3.25}$$

$$\zeta_{el} = \frac{\psi_{el} r_{el}^3}{\psi_{ed} r_{ed}^3 + \psi_{el} r_{el}^3} \tag{3.26}$$

The volume fraction of the electrolyte and electrode particle with respect to the solid phase can be calculated as:

$$\psi_{ed} = \frac{\phi_{ed}}{\phi_{ed} + \phi_{el}} \tag{3.27}$$

$$\psi_{el} = \frac{\phi_{el}}{\phi_{ed} + \phi_{el}} \tag{3.28}$$

3.3.3 Current generation

By using the Butler-Volmer equation (3.29), we can calculate the current density i at any point in the cathode and anode.

$$i = i_0 \left[exp\left(\frac{\alpha_a F \eta_{act}}{RT}\right) - exp\left(-\frac{\alpha_c F \eta_{act}}{RT}\right) \right] \tag{3.29}$$

where i_0 =Exchange current density for hydrogen oxidation or oxygen reduction reactions
η_{act} =Activation overpotential

$$\eta_{act,a} = E_a - E_a^{eq} \tag{3.30}$$

$$\eta_{act,c} = E_c - E_c^{eq} \tag{3.31}$$

where

$$E_a^{eq} = \frac{\mu_{H_2O}^o - \mu_{H_2}^o}{2F} + \frac{RT}{2F} ln \frac{p_{H_2O,a}}{p_{H_2,a}} \tag{3.32}$$

$$E_c^{eq} = \frac{\mu_{O_2}^o}{4F} + \frac{RT}{4F} ln(p_{O_2,c}) \tag{3.33}$$

In this form of the Butler-Volmer equation, the exchange current density i_0 is a function of local concentration and temperature at the reaction sites.

This work uses the expressions given by Zhu and Kee [27, 28] for exchange current density on both the anode and cathode sides.

$$i_{o,a} = i_{H_2}^* \frac{(p_{H_2}/p_{H_2}^*)^{\frac{\alpha_a - 1}{2}} (p_{H_2O}/p_{atm})^{\frac{\alpha_a}{2}}}{1 + (p_{H_2}/p_{H_2}^*)^{1/4}} \tag{3.34}$$

where $i_{H_2}^*$ is the exchange current density and from [27] is $4800 A/cm^3$ for anode and $56000 A/cm^3$ for cathode. $p_{H_2}^*$ is defined as:

$$p_{H_2}^* = \frac{A_{des}\Gamma^2\sqrt{2\pi RTW_{H_2}}}{\gamma_o} exp\left(-\frac{E_{des}}{RT}\right) \tag{3.35}$$

where $A_{des} = 5.59 \times 10^{19}$ s.cm^2/mol is pre exponential factor for the hydrogen desorption reaction, $\Gamma = 2.6 \times 10^{-9}$ is surface site density, $E_{des} = 88.12$ kJ/mol is activation energy

$i_{o,c}$ is define as

$$i_{o,c} = i_{O_2}^* \frac{(p_{O_2}/p_{O_2}^*)^{\frac{\alpha_a}{2}}}{1 + (p_{O_2}/p_{O_2}^*)^{1/2}} \tag{3.36}$$

$p_{O_2}^*$ is defined as

$$p_{O_2}^* = A_{O_2} exp\left(-\frac{E_{O_2}}{RT}\right) \tag{3.37}$$

$i_{O_2}^*$ is the exchange current factor for the cathode current density, $A_{O_2} = 4.9 \times 10^8$ atm is the pre-exponential factor for the O_2 desorption reaction on LSM, $E_{O_2} = 200$ kJ/mol is the activation energy for the oxygen desorption reaction.

Table 3.1: Simulation conditions used in the porous anode model

Parameter	**Value**	**Units**
Operating Temperature	1073	K
Operating Pressure	1	atm
H_2 mole fraction , x_{H2}, in	0.97	
H_2O mole fraction , x_{H2}, in	0.03	
O_2 inlet mole fraction x_{O2}, in	0.21	
N_2 inlet mole fraction x_{N2}, in	0.79	
Mean inlet fuel mass flow rate, m°, in	1.67×10^{-7}	kg/s
Mean inlet air mass flow rate, m°, in	1.77×10^{-6}	kg/s

Table 3.2: Parameters used in the model

Parameter	**Value**	**Units**
Anode		
Thickness	550	μm
Exchange current factor	8.5	A/cm^2
YSZ Particle radius	0.5	μm
Ni Particle radius	0.5	μm
Porosity	0.35	
Anode Symmetric factor(α_a)	1.5	
Cathode Symmetric factor(α_c)	0.5	
Permeability of anode	1.97×10^{-11}	m^2
Cathode		
Thickness	50	μm
Exchange current factor	2.8	A/cm^2
YSZ Particle radius	0.25	μm
LSM Particle radius	0.75	μm
Porosity	0.35	
Anode Symmetric factor(α_a)	0.75	
Cathode Symmetric factor(α_c)	0.5	
Permeability of cathode	1.957×10^{-11}	m^2
Electrolyte		
Thickness	20	μm

3.4 Solver and meshing

The creation of geometries, meshing, and simulation is performed using COMSOL Multiphysics 4.2a [6]. The postprocessing is done in both COMSOL as well as MATLAB.

We use a mapped mesh and the mesh density is controlled by specifying the number of grid point at the relevant boundaries of the electrodes, electrolyte, and channels. The mesh distribution is shown in figures 3.4 and 3.3.

Mesh

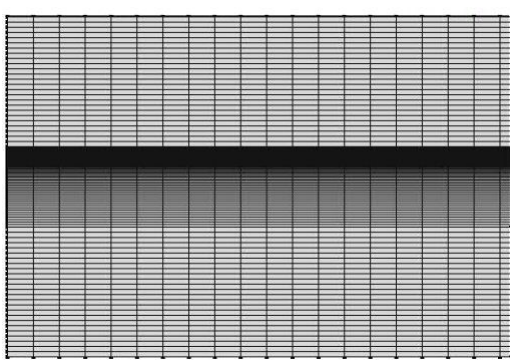

Figure 3.3: Mesh for 2D geometry

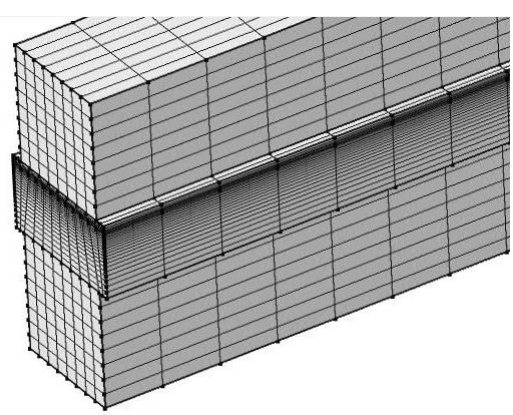

Figure 3.4: Mesh for 2D geometry

For the mesh used in the 3D model, the maximum and minimum element sizes were 5 and 0.9 mm respectively. The 3D model was only used for a limited number of simulations as the computational load became unmanagable for meshes that were finer than the above specified sizes. Thus, the 3D simulations are limited to the case of current generation only at the electrode-electrolyte boundaries.

In the 2D model, the maximum and minimum element sizes were 0.2 mm and 0.015 mm respectively along the length of the cell. The solutions were quite sensitive to the mesh element sizes perpendicular to the electrode-electrolyte boundaries. For the mesh converged results, the mesh element sizes perpendicular to the electrode-electrolyte boundaries varied from 1–20 μm in the anode and 1–5 μm in the cathode with the thinnest elements being at the electrode-electrolyte boundary. The mesh used for 2D models consists of over 30750 elements.

Within COMSOL, we mostly use default settings while solving these models except for a tighter relative tolerance of 10^{-4}. The segregated solver is used as memory requirements are prohibitive for the direct, fully coupled solver. The solution is obtained by iteratively solving each physics in turn until the overall error is within the given tolerance limits.

Chapter 4

Results and discussion

Results are presented for 3D and 2D models both of which represent an anode supported planar SOFC as described in the previous chapter. Both models include: flow and mass transfer in the air and fuel channels as well as the electrodes as well as electronic and ionic charge transport in the electrodes and electrolyte. All results are for isothermal operation at $800°C$.

4.1 Results from 3D model: current generation only at electrode-electrolyte boundaries

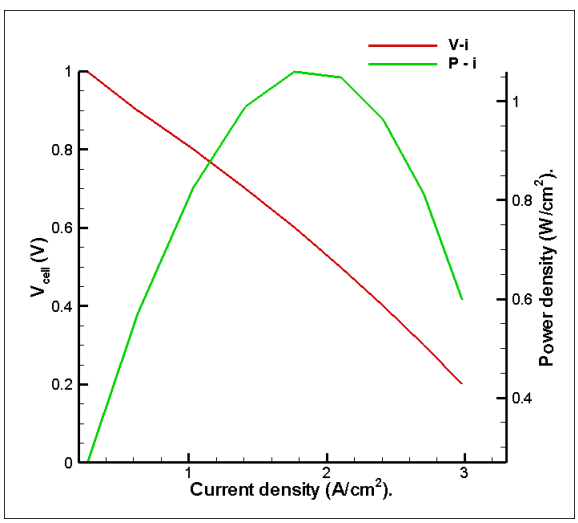

Figure 4.1: Voltage and power density *vs* current density curves for 3D model. $x_{H_2,in} = 0.97$, $x_{H_2O,in} = 0.03$.

Figure 4.1 gives the voltage and power density *vs* current density curves for the base case. The power density curve is constructed from i-V curve by multiplying the voltage at each point on the i-V curve by the corresponding current density. Performance that is typical for an SOFC is seen

for the $V - i$ as well as $P - i$ plots where the cell voltage decreases almost linearly with current density. Power density increases with increasing current density, reaches a maximum, and then falls at higher current densities due to the drop in the cell voltage.

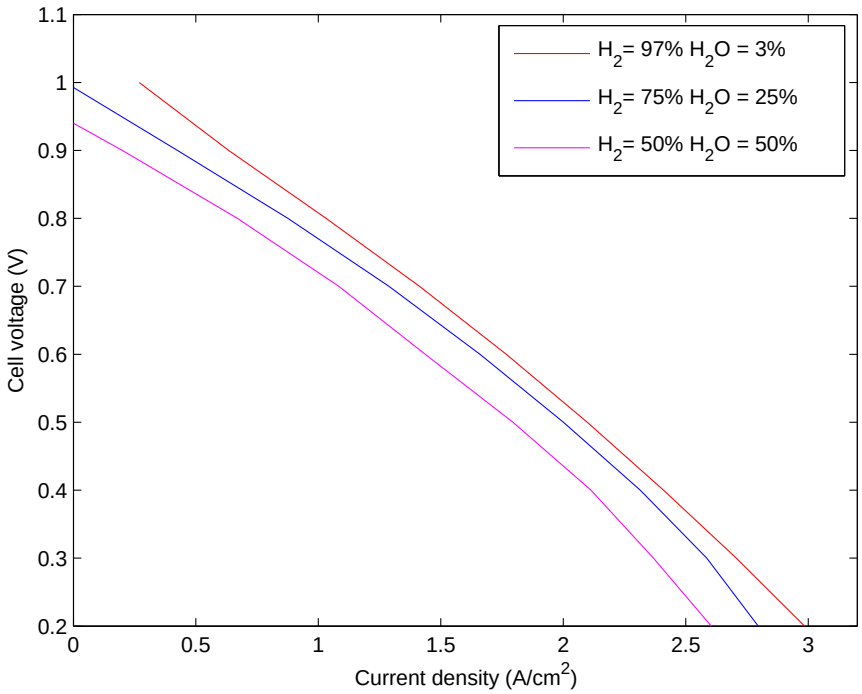

Figure 4.2: Effect of changing H_2 and H_2O content in fuel.

Figure 4.2 shows the effect of changing hydrogen and water composition with $x_{H_2,in}+x_{H_2O,in} = 1$. One can clearly see the change in OCV and the $V-i$ curve shifts down with decreasing hydrogen content in the fuel. The OCV is not imposed using the Nernst equation but comes out naturally as the cell voltage where the net current is zero. This is possible because of the thermodynamically consistent development of the electrode potentials and current generation as given in section 3.3.3.

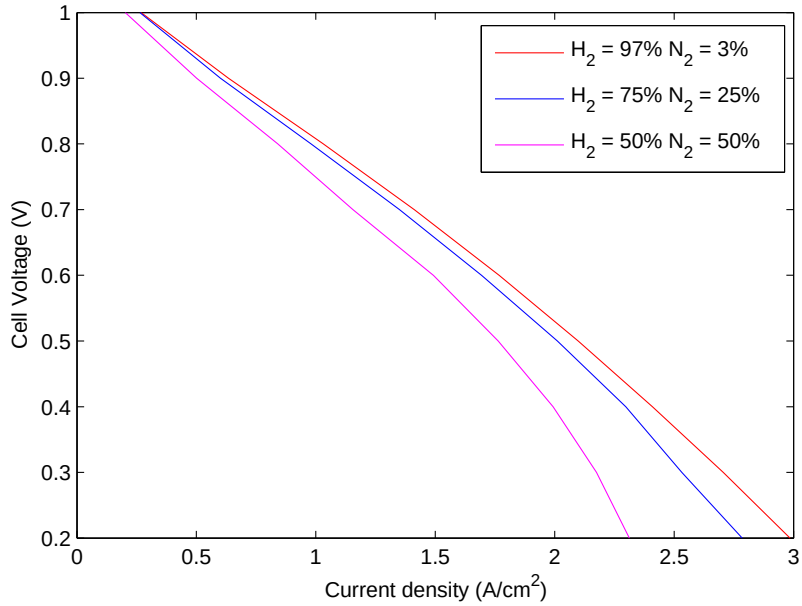

Figure 4.3: Effect of changing H_2 content in fuel, $x_{H_2O,in} = 0.03$.

Figure 4.3 shows the effect of changing hydrogen composition in the fuel inlet keeping the water content constant at $x_{H_2O,in} = 0.03$. N_2 is added to the fuel to make up the balance as H_2 content is decreased. Again, one sees the change in OCV as expected. Unexpectedly, the performance is worse for the same $x_{H_2,in}$ than in figure 4.2. Thus, although the results in 4.2 have a higher water content, the performance is better even though water is a product of the reaction. This can however be explained by closely examining equation (3.29) where we see the equation for the exchange current density has a positive exponent for p_{H_2O}.

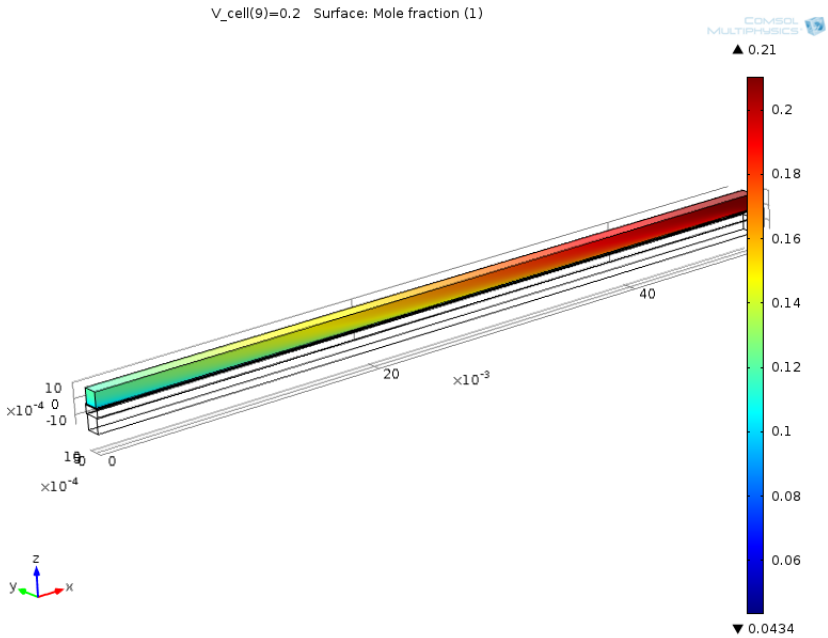

Figure 4.4: Oxygen concentration along the channel and electrode

Figures 4.4 and 4.5 give the reactant mole fractions along the channel length. One can clearly see the consumption of both O_2 and H_2 as they move along the channel from their respective inlets to the outlets.

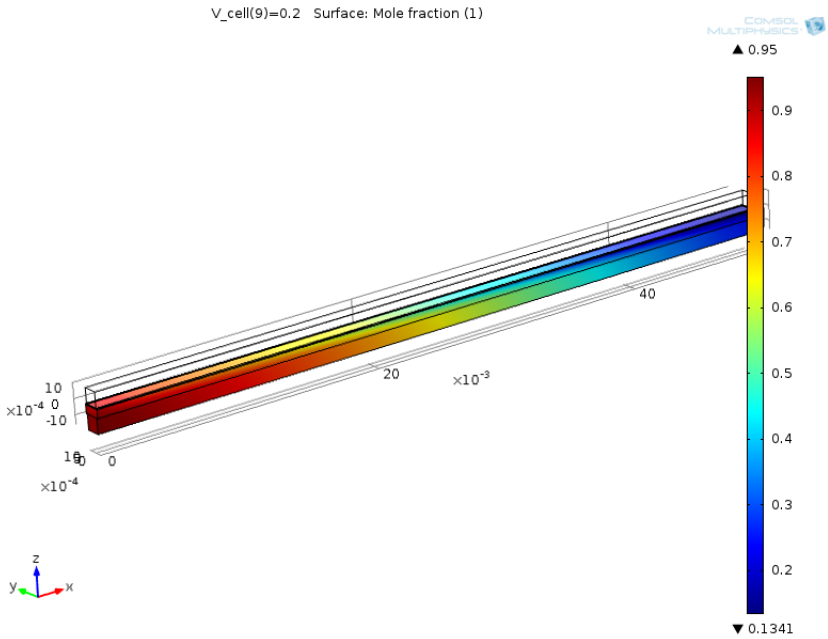

Figure 4.5: Hydrogen concentration along the channel and electrode

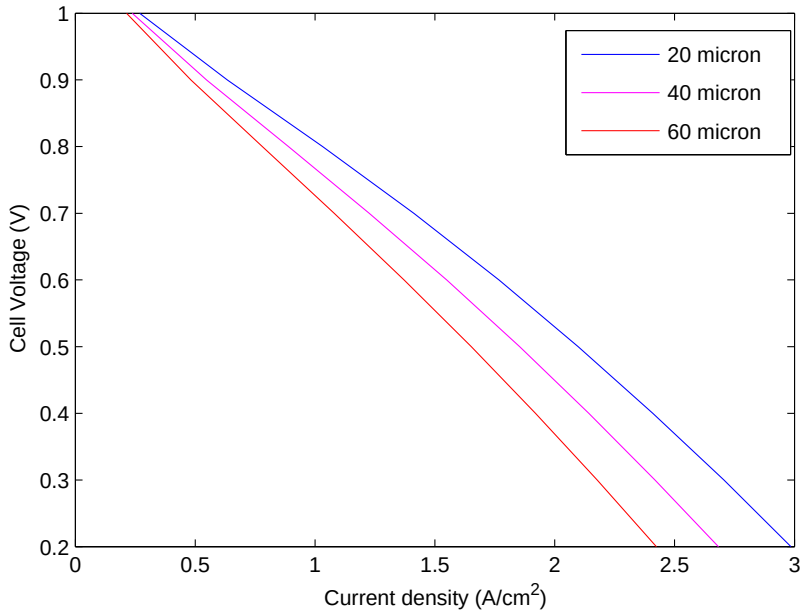

Figure 4.6: Changing electrolyte thickness

Figure 4.6 shows the effect of increasing the electrolyte thickness. The consequent increase in ohmic losses leads to a decrease in current density at any particular cell voltage.

4.2 2D model results: current generation throughout electrodes

All practical SOFC electrodes are mixed ionic-electronic conductors to maximize the three phase boundary (tpb) available for reaction. This implies that the current generation is distributed throughout the electrodes. As mentioned before, the 2D model was developed in this work because the mesh sizes required for accurately resolving current generation in composite electrodes led to a 3D model that was too computationally expensive to solve with our resources.

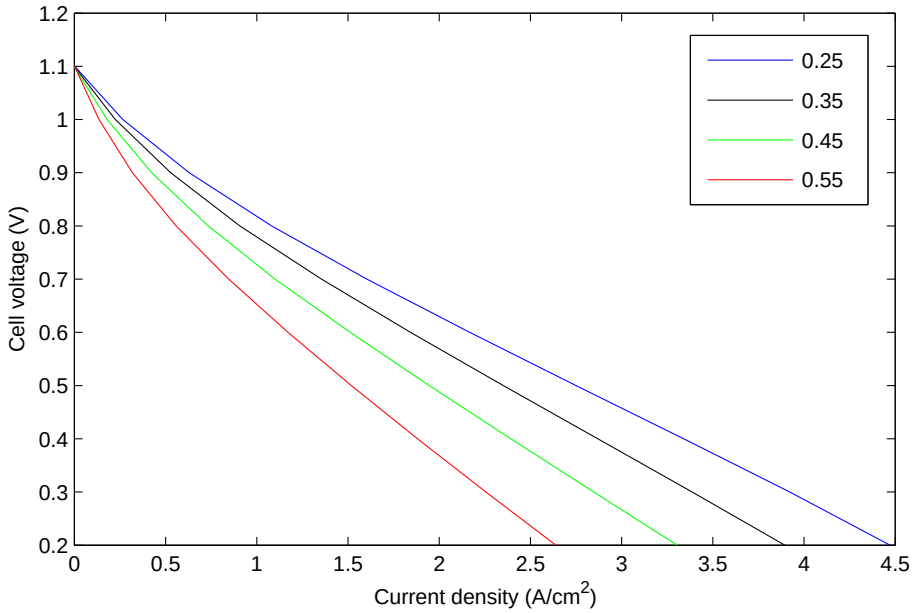

Figure 4.7: Effect of changing electrode porosity on cell performance. Inlet composition of fuel: 97% H_2 and 3% H_2O.

Figure 4.7 shows the effect of changing porosity simultaneously for the cathode and anode. The results seem counter-intuitive as the effective diffusivity as well as the permeability is expected to decrease with a decrease in porosity. This predicted increase in the mass transfer resistance is possibly overshadowed by the much greater effect of increase in effective ionic conductivity and volumetric tpb density. An increase in effective ionic conductivity leads to an increase in the active volume in an electrode. Additionally, an increase in tpb density also leads to an increase in the exchange current density as i_k^* in equations (3.34) and (3.36) is directly proportional to tpb density. This effect needs to further examined before any conclusions can be drawn.

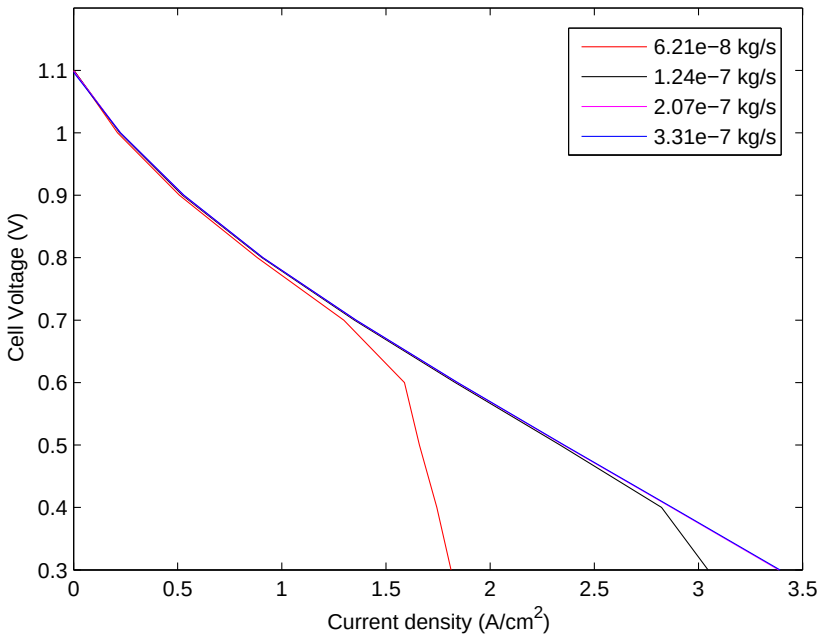

Figure 4.8: Effect of changing fuel flow rate on $V - i$ performance. Inlet composition of fuel: 97% H_2 and 3% H_2O.

Figure 4.8 shows the effect of changing fuel flowrate on overall $V - i$ performance curves. The $V - i$ curves indicate no significant effect until the flow-rate falls below a critical value after which, mass transport limitations give a sharp drop in performance at $i > 1.5A/cm^2$.

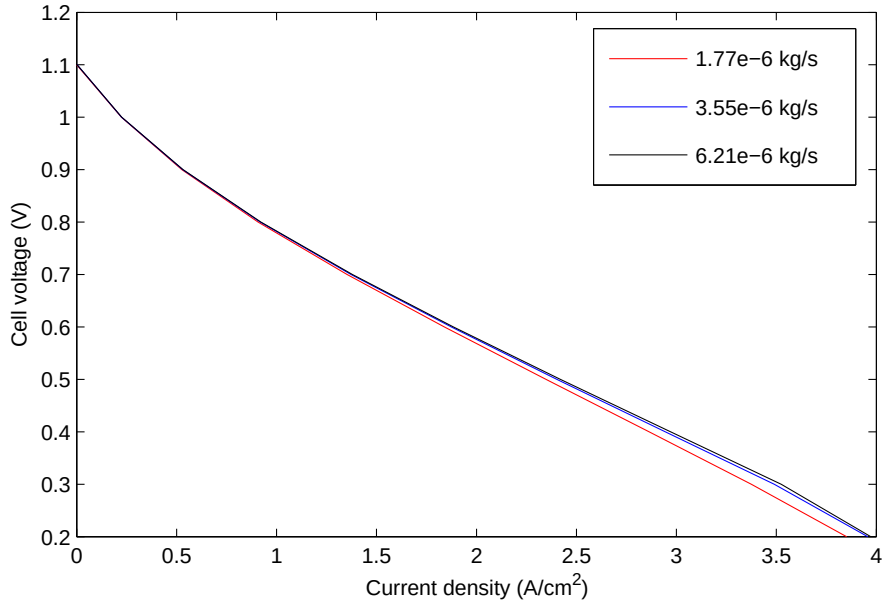

Figure 4.9: Different air flow rate

Figure 4.9 shows the effect of changing air flow-rate on $V - i$ curves. For the flow-rates examined, the $V - i$ curves do not show a significant effect which essentially means that the flow-rates are high enough to avoid mass transfer limitations in the cathode.

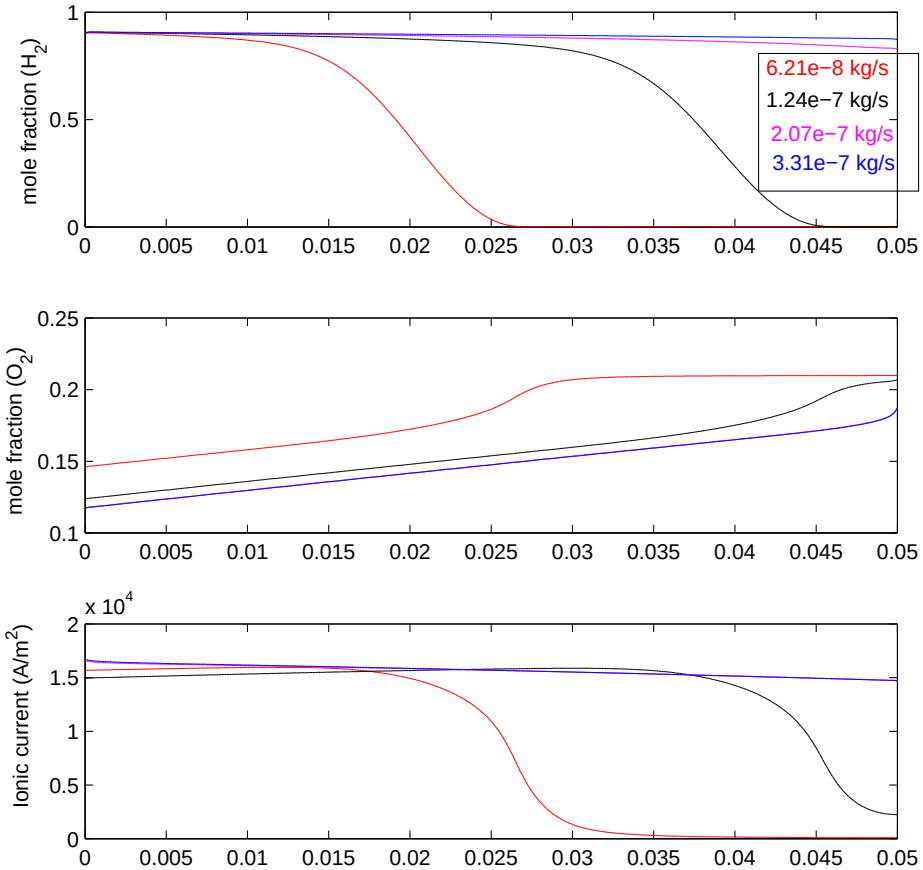

Figure 4.10: x_{H_2}in fuel, x_{O_2} in air, and i profiles along the length of the cell. $V_{cell} = 0.3V$; counter-flow of air and fuel. Inlet composition of fuel: 97% H_2 and 3% H_2O.

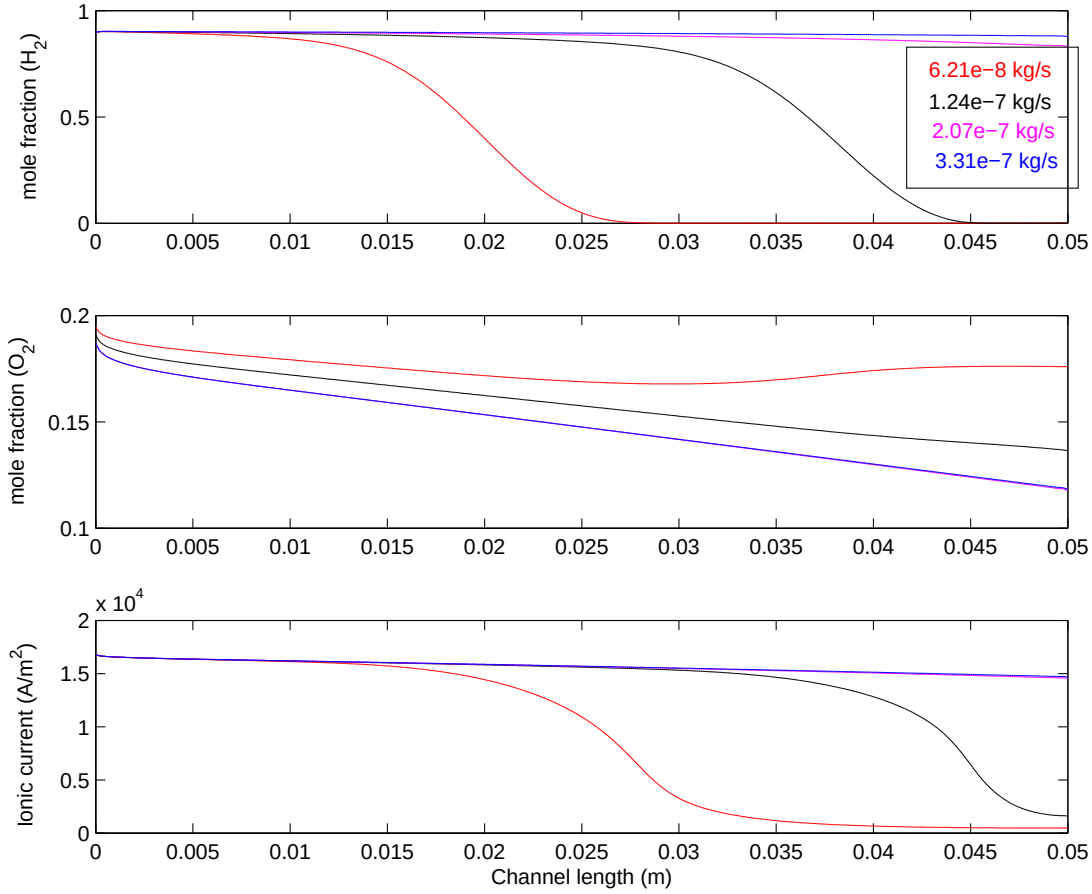

Figure 4.11: x_{H_2}in fuel, x_{O_2} in air, and i profiles along the length of the cell. $V_{cell} = 0.3V$; co-flow of air and fuel. Inlet composition of fuel: 97% H_2 and 3% H_2O.

Figures 4.10 and 4.11 give the profiles of x_{H_2} at the anode-electrolyte interface, x_{O_2} at the cathode-electrolyte interface, and i_{ionic} in the electrolyte for four different fuel flow-rates at an operating cell voltage of 0.3 V. One can see the effect of decreasing fuel flow-rate which leads to the H_2 content of the fuel dropping drastically within a short distance for the two lower fuel flowrates. At the lowest fuel flowrate, the effect on the O_2 mole fraction profile underlines the counterflow arrangment and as the fuel runs out by the middle of the fuel cell. The current generation also drops dramatically for the fuel starved section.

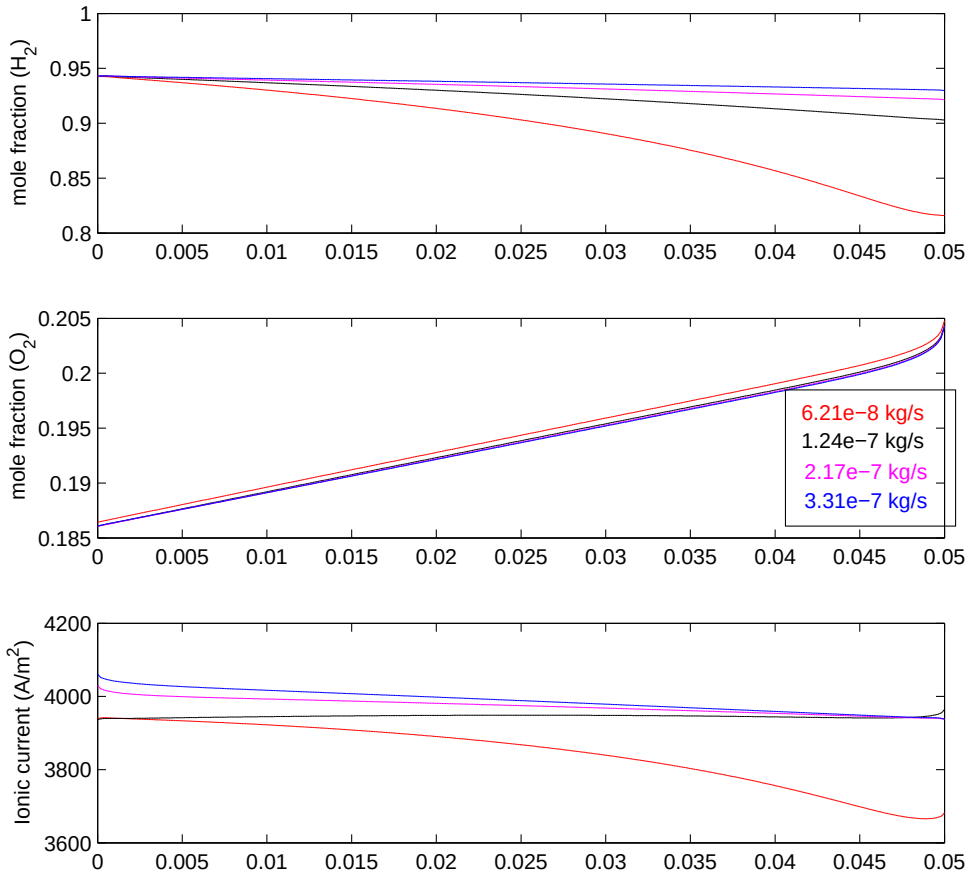

Figure 4.12: x_{H_2}in fuel, x_{O_2} in air, and i profiles along the length of the cell. $V_{cell} = 0.8V$; counter-flow of air and fuel. Inlet composition of fuel: 97% H_2 and 3% H_2O.

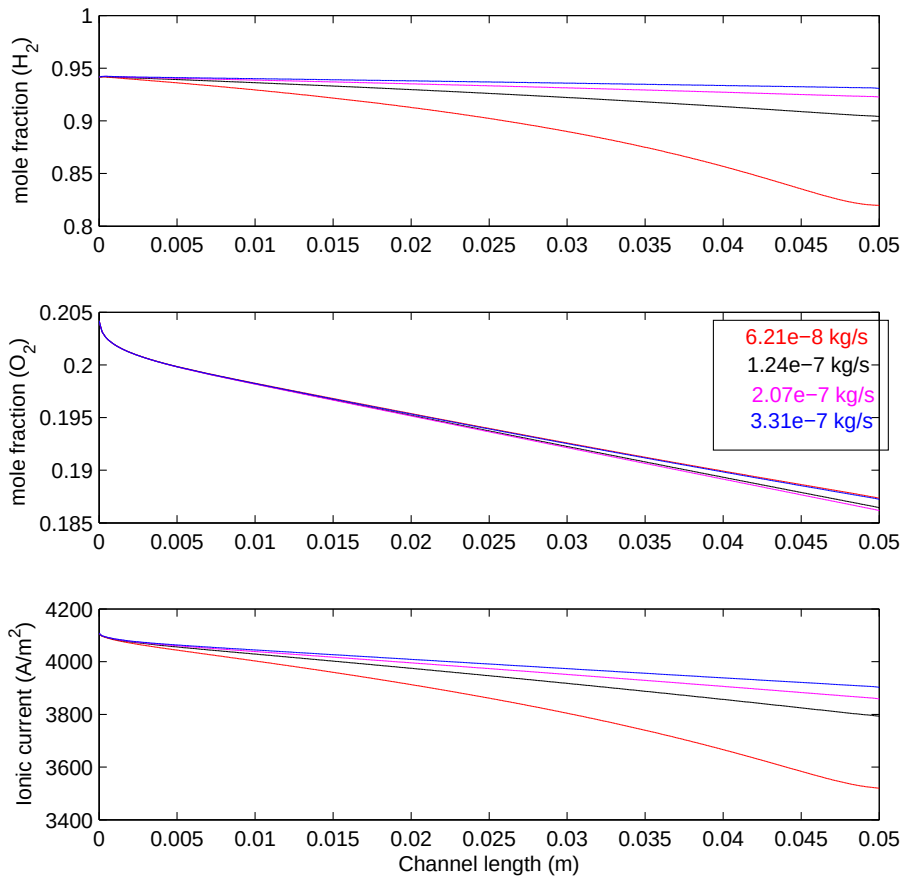

Figure 4.13: x_{H_2}in fuel, x_{O_2} in air, and i profiles along the length of the cell. $V_{cell} = 0.8V$; co-flow of air and fuel. Inlet composition of fuel: 97% H_2 and 3% H_2O.

Figures 4.12 and 4.13 are the same variables as above but plotted at a more reasonable cell voltage of 0.8 V. Note the reduction in current generation which is $\approx 4000A/m^2$ at 0.8 V as opposed to $\approx 15000A/m^2$ at 0.3 V (when the fuel flow-rate is adequate).

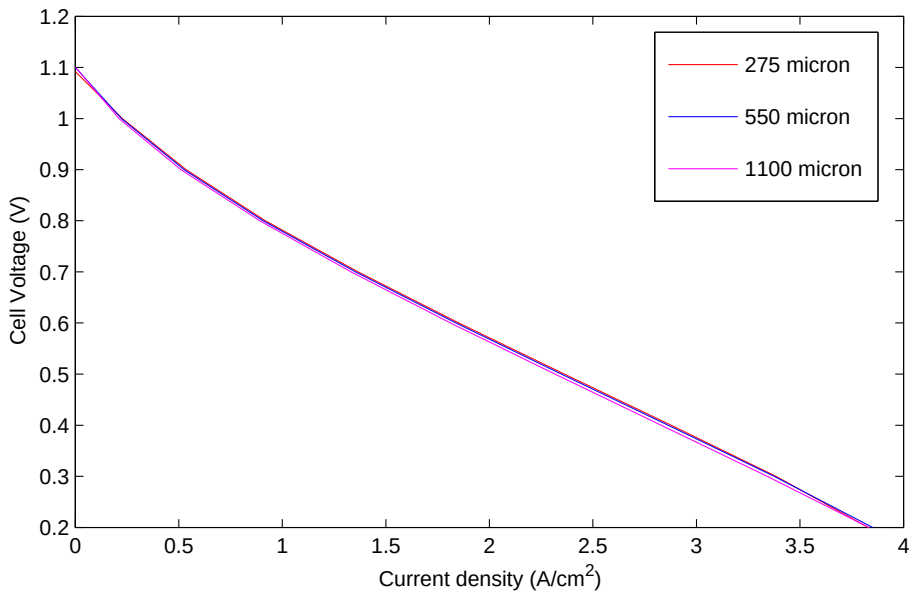

Figure 4.14: Cell performance as a function of anode thickness t_{anode}. Inlet composition of fuel: 97% H_2 and 3% H_2O.

The final set of results are given in figures 4.14 and 4.15 where the effect of changing electrode thickness is examined. For the chosen anode supported design, doubling or halving the standard chosen value for $t_{anode} = 550\mu m$ has essentially no impact on performance. The standard value of about half a mm is in fact required for provinding structural support to the fuel cell. On the other hand, halving the $t_{cathode}$ from $50\mu m$ to $25\mu m$ causes a measureable reduction in the current generation. Doubling the $t_{cathode}$ to $100\mu m$ increases current generation somewhat as well. Thus, it seems there is some scope for optimizing the cathode thickness for improved performance.

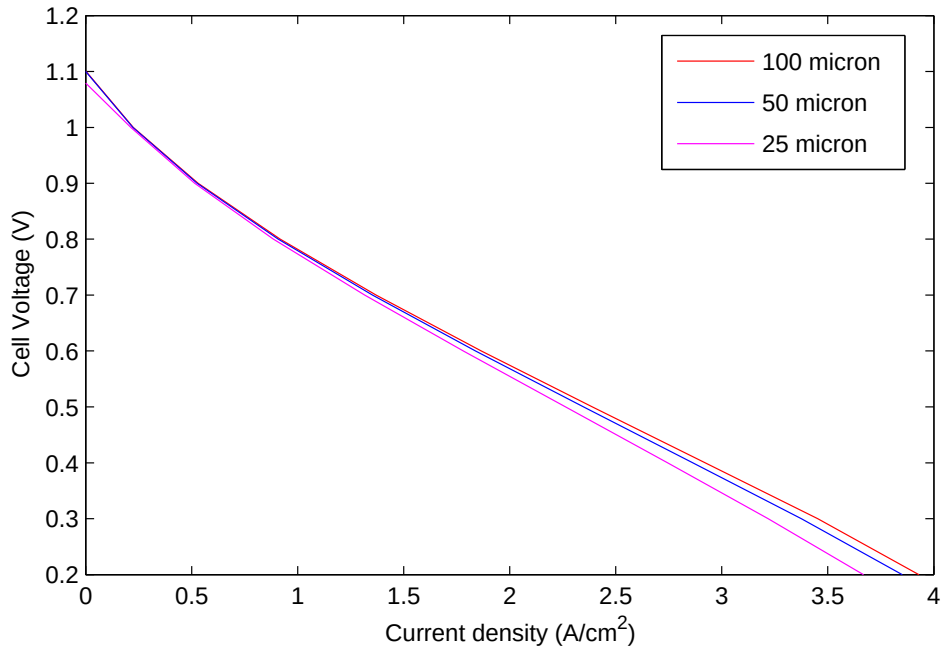

Figure 4.15: Cell performance as a function of cathode thickness t_{anode}. Inlet composition of fuel: 97% H_2 and 3% H_2O.

Chapter 5

Conclusions

This work presents 2D and 3D multiphysics models for a planar anode-supported SOFC. The physical phenomena that are explicitly modeled include fluid flow, mass transfer, and charge transport. The results obtained from simulations of these two models are examined for correctness by verifying expected trends in performance upon varying key operating conditions such as inlet gas composition as well as structural parameters such as electrolyte thickness.

Having verified the model, we run a limited set of parametric studies that examine the effect of varying fuel and air flow-rates as well as anode and cathode thickness. The following can be concluded from this study:

- Fuel and air flow-rate effects are explainable by analyzing the composition profiles along the length of the SOFC. These profiles clearly demonstrate mass transfer limitations due to fuel starvation at low flow-rates. Similar behavior is expected for air flow-rate as well although usually there is little need for limiting air flow.
- There seems to be scope for optimizing cathode thickness as a doubling of thickness leads to a measurable increase in $V - i$ performance.

Future work

A suggestion for future work would be a more extensive parametric study to look for better optimized design. Another possible direction is to compare the detailed model given here with simpler models such as the one given in [28] to examine the effect of model assumptions. Another extension would be to include heat transfer into the models developed here to examine non-isothermal behaviour.

References

[1] Bear, J. *Dynamics of Fluids in Porous Media*, American Elsevier, New York, 1972.

[2] Bird, R. B., Stewart, W. E., and Lightfoot, E. N. *Transport Phenomena*, John Wiley & Sons, New York, U.S.A, 2nd edition, 2009.

[3] Bouvard, D., and Lange, F. F. Relation between percolation and particle coordination in binary powder mixtures *Acta Metall. Mater* **39**, 3083-3090, 1991.

[4] Chen, D., He, H., Zhang, D., Wang, H, and Ni, M. Percolation Theory in Solid Oxide Fuel Cell Composite Electrodes with a Mixed Electronic and Ionic Conductor. *Energies* **6**, 1632-1656, 2013.

[5] Chen, D., Zijing, Zhu, H., Kee, R. J. Modeling and control of solid oxide fuel cell system, *Journal of Power Sources* **196**, 197-207, 2011.

[6] COMSOL. COMSOL Multiphysics help documentation, COMSOL 4.2a, 2011.

[7] Cussler, E. L. Diffusion: Mass transfer in fluid systems, Cambridge University Press, Third edition, 2009.

[8] DiGiuseppe, G., Gowda, Y. J., Honnagondanahalli, N. K. A Two-Dimensional Modeling Study of a planar SOFC using actual cell testing geometry and operating conditions, *Journal of Fuel Cell Science and Technology* **9**, 011016-1, 2012.

[9] Hardjo, E. Numerical model of Ni-infiltrated porous anode solid oxide fuel cells, Queen's University Kingston, Ontario, Canada, October 2012.

[10] Hagiwara, A., Michibata, H., Kimura, A., Jaszcar, M. P., Tomlins, G. W., Veyo, S. E. Tubular solid oxide fuel cell life tests *Third International Fuel Cell Conference* **D2**, 365-368, 1999.

[11] Hirano, A., Suzuki, M., Lppommatsu M. Evaluation of a New Solid Oxide Fuel Cell System by Nonisothermal Modeling *Journal of The Electrochemical Society* **139**, 2744-2751, 1992.

[12] Kee, R. J., Zhu, H., and Goodwin, D. G. *International Symposium on Combustion*, July 2004.

[13] Kenney, B., Valdmanis, M., Baker, C., Pharoah, J. G., Karan, K. Computational of TPB length, surface area and pore size from numerical reconstruction of composite solid oxide fuel cell electrodes, *Journal of Power Sources* **189**, 1051-1059, 2009.

[14] Li, P. W., Chyu, M. K. Simulation of the chemical/electrochemical reactions and heat/mass transfer for a tubular SOFC in a stack, *Journal of Power Sources* **124**, 487-498, 2003.

[15] Lmno Engg. Gas Viscosity *http://www.lmnoeng.com/Flow/GasViscosity.htm*, accessed 20-Feb-2012.

[16] Monder, D. S. *Modelling studies for H_2S fuelled SOFCs.* PhD thesis, University of Alberta, Edmonton, Canada, 2008.

[17] Monder, D. S., Chuang, T. K., and Nandakumar, K. A Fully Coupled Multiphysics Model for a H_2S SOFC, *Journal of The Electrochemical Society*, **157**(4), B542-B551, 2010.

[18] O'Hayre, R., Cha, W. S., Colella, W., Prinz, B. F. *Fuel Cell Fundamentals*, John Wiley Sons, 2nd edition, 2009.

[19] Sanyal, J., Goldin, G. M., Zhu, H., Kee, R. J. A particle-based model for predicting the effective conductivity of composite electrodes. *Journal of Power Sources* **195**, 6671-6679, 2010.

[20] Singhal, S. C. Progress in Tubular Solid Oxide Fuel Cell Technology, *Electrochemical Society Proceedings* **19-99**, 39-51, 1999.

[21] Singhal, S. C. Advances in solid oxide fuel cell technology, *Solid State Ionics* **135**, 305-313, 2000.

[22] Suwanwarangkul, R., Croiset, E., Fowler, M. W., Douglas, P. L., Entchev, E., Douglas, M. A. Performance comparison of Fick's, Dusty-gas and Stefan-Maxwell model to predict the concentration overpotential of a SOFC anode, *Journal of Power Sources* **122**, 9-18, 2003.

[23] Suzuki, M., Oshima, T. Co-ordination number of a multi-component randomly packed bed of spheres with size distribution, *Powder Technol.* **44**, 213-218, 1985.

[24] Tomlins, G. W., Jaszar, M. P. *Third International Fuel Cell Conference* **D2-4**, 369-372, 1999.

[25] Wilson J. R., and Barnett, S. A. Solid Oxide Fuel Cell Ni-YSZ Anodes; Effect of Composition on Microstructure and performance, *Electrochemical and Solid-State Letters* **11**, B181-B185, 2010.

[26] Wikipedia, Fuel cell *http://en.wikipedia.org/wiki/Fuel cell*, accessed 5-June-2012.

[27] Zhu, H., Kee, R. J., Janardhanan, V. M., Deutschmann, O, and Goodwin, D. G. Modeling Elementary Heterogeneous Chemistry and Electrochemistry in Solid-Oxide Fuel Cells, *Journal of The Electrochemical Society* **152** (12), A2427-A2440, 2005.

[28] Zhu, H., and Kee, R. J. Modeling Distributed Charge-Transfer Process in SOFC Membrane Electrode Assemblies, *Journal of The Electrochemical Society* **155** (7), B715-B729, 2008.